

Polarity and Twist Rate Detection for Accurate and Reliable Low Loss Multicore Fiber Fusion Splicing

Tristan Kremp⁽¹⁾, Yue Liang⁽²⁾, Alan H. McCurdy⁽²⁾

⁽¹⁾ OFS Laboratories, Somerset, NJ, USA; ⁽²⁾ OFS Fitel, LLC, Norcross, GA, USA

Author e-mail address: tkremp@ofsoptics.com

Abstract: Using a novel azimuthal alignment algorithm and side-view images, we reliably determine the polarity and twist rate of multicore fiber and achieve average losses as low as 0.03 dB using a 3-electrode arc-discharging fusion splicer. © 2022 The Author(s).

1. Introduction

While bandwidth demands continue to grow exponentially, multicore fiber (MCF) allows to increase the density of optical channels in the available space, e.g., in the ducts of hyperscale data centers or inside the armored protection layer of submarine communication cables. For the deployment of optical fiber and cable, fusion splicing of opposing fiber ends is a crucial step to maintain low insertion loss. While the lowest previously reported splice losses for MCF were ranging from 0.08 dB to 0.2 dB [1–8], we recently developed a novel azimuthal alignment algorithm and achieved an average passive splice loss in 4-core MCF of less than 0.03 dB [9] with a 3-electrode arc-discharging fusion splicer [10]. This is at the same level as typical single-core fiber splice losses, which are usually below 0.03 dB for active core alignment and around 0.04 dB for active cladding alignment.

However, MCF fusion splicing not only needs to provide low insertion loss, but also has to guarantee that the two opposing fiber ends are correctly aligned without confusing cores, i.e., transmission signal channels. This can be achieved by comparing in both fiber ends the location of a so-called marker, which is usually a small core-like refractive index change (see Fig. 1a), but can as well be an asymmetry such as a D-shape of the surrounding cladding. Since the marker is located at an asymmetric position (see Fig. 2), it not only allows to distinguish cores, but also to distinguish the two ends even of a single MCF. This binary piece of information is often referred to as the polarity of the fiber, which we here refer to with the values “+1” and “-1”. We define the core numbers such that they increase clockwise on the “+1” end and counterclockwise on the other end (“-1”). When splicing two ends of different fibers, their absolute polarities can either be different (“correct” relative polarity “+1”) or identical (“wrong” relative polarity “-1”), see Fig. 2.

Furthermore, in applications such as 3D shape sensing [11], the fiber cores may be subject to significant twist that needs to be quantitatively taken into account in side-view-based imaging to achieve the lowest possible splice loss. In this work, we therefore generalize the algorithm from [9] to also determine the twist rate, relative and absolute polarity of the two fiber ends in a side-view-based fusion splicer. In addition to very low average splice loss, we thus achieve an accurate twist rate detection with standard deviation < 2.5/m and a >95% reliable polarity detection.

2. Side-view images, sinograms and algorithm for polarity and twist rate detection

In the present study, we use the Fitel S185PM ROF fusion splicer hardware [10] and MCF with 4 cores (“4CF”) and 7 cores (“7CF”). End-view and side-view images before and after alignment and fusion splicing are shown in Fig. 1.

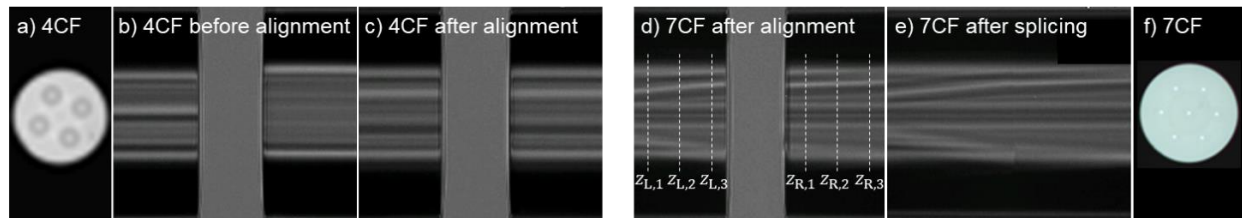


Fig. 1. (a) End-view of 4CF. (b,c) Side-view of two ends of untwisted 4CF before and after azimuthal alignment. (d,e) Side-view of two ends of 7CF with twist rates of approximately 100/m and 50/m, respectively, after alignment and fusion splicing, showing a perfect match despite the kink in the middle due to the different twist rates. (f) End-view of 7CF.

In the following, the angle ϑ denotes the azimuthal orientation of the fiber relative to the splicer camera plane in Fig. 1(b-e), z is the longitudinal location along the fiber, and x is the transverse coordinate parallel to the camera plane (x, z). Thus, Figs. 1b-e show the side-view intensity $I(\vartheta, x, z)$ for one fixed orientation of the two fibers to be spliced. Choosing instead a fixed location, e.g., $z = z_L$ close to the end of the left fiber, a side-view sinogram is the function $I(\vartheta, x, z_L)$ as shown in Fig. 3a, which is a series of cross-sectional intensity scans at different azimuthal orientations.

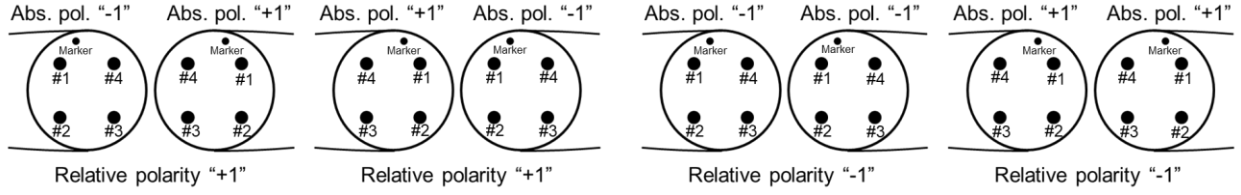


Fig. 2. Absolute and relative polarity conventions in the example of 4CF. If a clockwise rotation of the marker brings the marker closer to the closest core, then the absolute polarity is “+1”, otherwise “-1”. If two opposing fiber ends have different absolute polarities, then their relative polarity is “+1”, otherwise “-1”.

Correlating side-view sinograms that are taken near the ends $z = z_L$ and $z = z_R$ of the left and right fiber to be spliced, and integrating over the transverse coordinate x , we define the (global) cross-correlation

$$c(\vartheta) = \iint I(\vartheta', x, z_L) I(\vartheta' + \vartheta, x, z_R) d\vartheta' dx \quad (1)$$

The azimuthal spacing of the cores of 4CF (see Fig. 1a) is 90 degrees, similar to the fibers used in [1,4–6]. Hence, there are $M_{\text{equiv}} = 4$ equivalent ways (sectors, in this case quadrants) of aligning its cores before splicing. The cross-correlation $c(\vartheta)$ from Eq. (1) shown in Fig. 3b therefore has four distinct peaks in this case of the 4CF. Since a marker is usually small compared to the cores, it has only a minor impact on the height of these peaks.

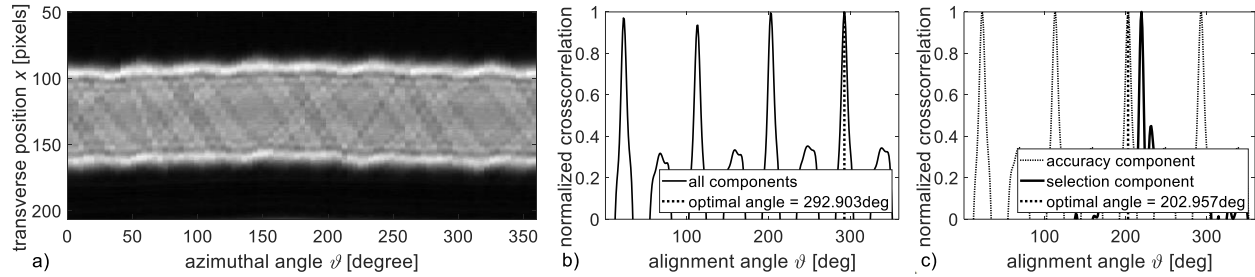


Fig. 3. (a) Side-view sinogram $I(\vartheta, x, z_L)$ of 4CF, left fiber. (b) Global normalized cross-correlation $c(\vartheta)$ of two ends of 4CF, leading to wrong quadrant. (c) Normalized cross-correlation separated into accuracy and selection component, leading to correct quadrant.

To get a more robust signal from the marker, we separate the (Fast) Fourier Transform vector \tilde{c} of the cross-correlation $c(\vartheta)$ into an accuracy (cores) component $\tilde{c}^{(\text{acc})}$ and a selection (marker, asymmetries) component $\tilde{c}^{(\text{sel})}$ according to

$$\tilde{c} = \tilde{c}^{(\text{acc})} + \tilde{c}^{(\text{sel})}. \quad (2)$$

We choose the accuracy component vector $\tilde{c}^{(\text{acc})}$ such that its entries $\tilde{c}_n^{(\text{acc})}$ are either zero or identical to the corresponding entries \tilde{c}_n of the global cross-correlation at all integer multiples of the fundamental frequency M_{equiv} ,

$$\tilde{c}_n^{(\text{acc})} = \tilde{c}_n \quad \text{if } n \in I^{(\text{acc})}, \quad \text{with } I^{(\text{acc})} = \{mM_{\text{equiv}}\}_{m \in \mathbb{Z}} \quad (3)$$

being the index set that contains all integer multiples of M_{equiv} . We note that the DC component is \tilde{c}_0 , and aliasing limits the range of the integer n in Eq. (3). The inverse Fourier transform of $\tilde{c}^{(\text{acc})}$ (dotted in Fig. 3c) has the period $360^\circ/M_{\text{equiv}}$, i.e., it has in this case $M_{\text{equiv}} = 4$ peaks of exactly identical height. The accurate azimuthal alignment angle is the location (in this case 202.957°) of that peak of the accuracy component that is closest to the single peak of the inverse Fourier transform of $\tilde{c}^{(\text{sel})}$ (solid in Fig. 3c). Instead, the highest peak of the global cross-correlation $c(\vartheta)$ from Eq. (1) in Fig. 3b would have led us to the wrong quadrant (292.9°), i.e., a 90° error and core confusion.

The fact that the peak of the selection component in Fig. 3c does not coincide with one of the peaks of the accuracy component in Fig. 3c indicates that the markers of these two particular fiber ends are not aligned when the cores are aligned. The relative polarity in this case is therefore detected as wrong (“-1”), whereas (after flipping one of the two fibers) it would be detected as correct (“+1”) when the peak of the selection component in Fig. 3c had coincided with a peak of the accuracy component. Hence, the relative polarity is automatically determined as a byproduct of the above algorithm from Fig. 3c, and we found it to be correct with >99% reliability. To also compute the absolute polarity of each fiber end, we replace Eq. (1) by $c(\vartheta) = \iint I(\vartheta', x, z_j) d\vartheta' dx$ and perform the above formalism separately for both fiber ends [12]. As a result, we found >95% reliability of the absolute polarity computation.

To determine the twist rate of both fibers in the splicer, we evaluate Eqs. (1)-(3) at multiple locations z_L and z_R as indicated by the vertical dashed lines in Fig. 1d and use two linear fits for the location-dependent optimum rotation angles close to the two fiber ends. Found twist rates for fibers with different draw twist rates are shown in Fig. 4a, with standard deviations $<2.5/\text{m}$ allowing for a reliable identification of fibers with different twist rates.

After the alignment computation, which is performed on a laptop that is connected to the splicer, one or both fibers are rotated by the total computed amount. An example after alignment is shown in Fig. 1(c).

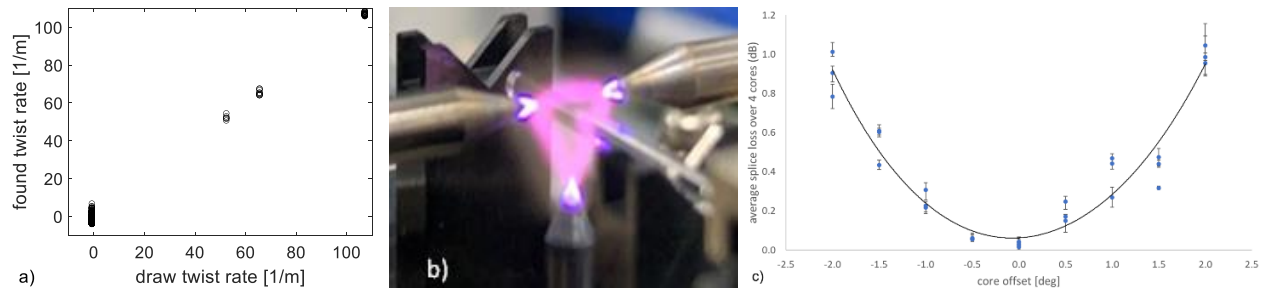


Fig. 4. (a) Twist rates found for 4CF and 7CF drawn at different twist rates. (b) 3-electrode splicing to achieve equal temperature and equally low loss for all cores. (c) Average splice loss of 4CF as a function of intentional rotational offset from the algorithm optimum.

3. Splice loss, speed and success rate

After the rotational alignment, the two fibers are fusion-spliced using the three-electrode arc-discharging S185PM ROF splicer [10] to achieve a uniform heat distribution across all cores, see Fig. 4b. The side-view sinogram scan, alignment computation, rotation and arc time amount to only about 90 seconds with our new splicing solution. We achieve an almost 100% alignment (correct core) success rate, and the resulting splice loss for 4CF at 1550nm wavelength is shown in Fig. 4c as a function of an intentional rotational offset. The measurement values at zero offset at the center of the curve in Fig. 4c confirm our recent result of <0.03 dB average splice loss [9], and the fact that no nonzero offset gives similarly low splice loss confirms the optimality of the computed rotation angle.

4. Conclusion

A novel azimuthal alignment algorithm is presented for multicore and other fibers that are not circularly symmetric, e.g., polarization-maintaining fibers. The cross-correlation of the side-view sinograms of the two fibers to be spliced is separated into an accuracy component and a selection component. The selection component is used to select the correct peak of the accuracy component, which is then used to accurately quantify the optimum alignment angle, as well as to identify the relative and absolute polarities of the two fibers with almost 100% reliability, respectively. The twist rate is computed by line fits to repeated measurements and computations at different longitudinal locations, with standard deviations of less than 2.5/m for a 7-core fiber. In combination with 3-electrode arc-discharging Fitel S185PM ROF splicer, we achieved an almost 100% alignment success rate with splicing times of only 90 seconds and single-core-fiber-like splice losses of less than 0.03 dB on average for a 4-core fiber design, regardless of polarity.

References

- [1] K. Saito, T. Sakamoto, T. Matsui, K. Nakajima and T. Kurashima, "Side-view based angle alignment technique for multi-core fiber," Optical Fiber Communications Conference (OFC), paper M3F.3, 2016, DOI: <https://doi.org/10.1364/OFC.2016.M3F.3>
- [2] W. Zheng, "Automated alignment and splicing for multicore fibers," Optical Fiber Communications Conference (OFC), paper OM3I.4, 2013, DOI: <https://doi.org/10.1364/OFC.2013.OM3I.4>
- [3] W. Zheng, D. Duke, T. Kubo, and B. Malinsky, "Interrelation profile analysis method for alignment of polarization-maintaining fiber," Optical Fiber Communications Conference (OFC), paper JThA61, 2010, DOI: <https://doi.org/10.1364/NFOEC.2010.JThA61>
- [4] M. Ohzeki, "Alignment and fusion splicing techniques for MCFs," European Conference on Optical Communication (ECOC), Workshop Mo1A-WS, 2021
- [5] M. Ohzeki, Y. Sasaki, K. Takenaga, K. Ichii and K. Aikawa, "Side-view rotational alignment method for trench-assisted 4-core fibers," Optical Fiber Communications Conference (OFC), paper M4E.4, 2022, DOI: <https://doi.org/10.1364/OFC.2022.M4E.4>
- [6] M. Takahashi, T. Fujii, R. Sugizaki, M. Tsukamoto and Y. Arashitani, "Field usable fusion splicing technique for multicore fiber," IEEE Photonics Society Summer Topicals Meeting (SUM), 2020, DOI: <https://doi.org/10.1109/SUM48678.2020.9161043>
- [7] W. Zheng, H. Sugawara and B. Malinsky, "Fourier analysis method for asymmetric polarization-maintaining fiber," Optical Fiber Communications Conference (OFC), paper JW2A.12, 2012, DOI: <https://doi.org/10.1364/NFOEC.2012.JW2A.12>
- [8] Y. Amma, A. Takahashi, K. Takenaga and S. Matsuo, "Accuracy of core alignment with end-view function for multicore fiber," IEEE Photonics Society Summer Topicals Meeting (SUM), 2014, DOI: <https://doi.org/10.1109/SUM.2014.94>
- [9] T. Kremp, Y. Liang and A. H. McCurdy, "Less than 0.03 dB multicore fiber passive fusion splicing using new azimuthal alignment algorithm and 3-electrode arc-discharging system," European Conference on Optical Communication (ECOC), paper Tu3A.3, 2022
- [10] <https://www.furukawa.co.jp/splicer/en/product/s185pmrof.html>
- [11] P. S. Westbrook et al., "Continuous multicore optical fiber grating arrays for distributed sensing applications," J. Lightwave Technol., vol. 35, no. 6, pp. 1248–1252, March 2017.
- [12] T. Kremp, Y. Liang and R. L. Lingle, International patent application WO2022/125443A1, published 16 June 2022.